Study of lattice thermal conductivity of alpha-zirconium by molecular dynamics simulation*

Wu Tian-Yu(武天宇), Lai Wen-Sheng(赖文生)†, and Fu Bao-Qin(付宝勤)

Laboratory of Advanced Materials, Department of Material Science and Engineering, Tsinghua University, Beijing 100084, *China*

(Received 11 August 2012; revised manuscript received 15 January 2013)

The non-equilibrium molecular dynamics method is adapted to calculate the phonon thermal conductivity of alpha-zirconium. By exchanging velocities of atoms in different regions, the stable heat flux and the temperature gradient are established to calculate the thermal conductivity. The phonon thermal conductivities under different conditions, such as different heat exchange frequencies, different temperatures, different crystallographic orientations, and crossing grain boundary (GB), are studied in detail with considering the finite size effect. It turns out that the phonon thermal conductivity decreases with the increase of temperature, and displays anisotropies along different crystallographic orientations. The phonon thermal conductivity in [0001] direction (close-packed plane) is largest, while the values in other two directions of $[2\bar{1}\bar{1}0]$ and $[01\bar{1}0]$ are relatively close. In the region near GB, there is a sharp temperature drop, and the phonon thermal conductivity is about one-tenth of that of the single crystal at 550 K, suggesting that the GB may act as a thermal barrier in the crystal.

Keywords: alpha-zirconium, lattice thermal conductivity, molecular dynamics simulation

PACS: 66.70.–f, 65.40.–b, 44.10.+i, 02.30.Em **DOI:** 10.1088/1674-1056/22/7/076601

1. Introduction

Alpha-zirconium and zircaloys have been widely employed in fuel cladding and pressure tubes in nuclear reactors. Understanding the mechanisms, which control the production, number, and arrangement of defects during irradiation in metals, is crucial to predicting and assessing the material performance in power reactor system. Molecular dynamics (MD) computer modeling has been demonstrated to be a valuable technique for dealing with these matters. Several studies of cascades in alpha-zirconium have been reported.[1–3] However, those papers did not consider the edge heat transport of the system, which is a factor influencing the accuracy of simulation results. Moreover, in MD simulations of radiation effects in solids, the sizes of models are limited by computer power. However, the boundary heat transportation obtained by the phonon conductivity can eliminate the effect of limited size model, which makes the MD simulations more realistic.

The thermal conductivity of alpha-zirconium at high temperature consists of two major contributions of electron conductivity and phonon conductivity.[4,5] According to Born–Oppenheimer approximation, electronic motion and nuclear motion, namely electronic dynamics and lattice dynamics can be considered separately. Properties such as thermal expansion, specific heat capacity of non-electronic contribution, and thermal conductivity of semiconductor and ceramic are determined by lattice dynamics, while electronic dynamics controls the properties of the conductivity, electronic thermal conductivity, and superconductivity. In the radiation damage process, the defect production is determined by the lattice dynamics rather than electronic dynamics, because the damage in solids is caused by the displacements of atoms through atomic collision (such as cascades). MD is a technology and tool for dealing with lattice dynamics, which has been widely used to simulate radiation damage and phonon thermal conductivity without considering electronic behavior.[6] As is well known, the electron thermal conductivity makes the main contribution to the total thermal conductivity in metal or alloy. The electron thermal conductivity plays a predominant role in heat transportation in the case of thermal contact, yet it has a little influence on the defect production if the electron thermal energy does not convert into the atomic kinetic energy. As both the radiation damage process and the phonon thermal conductivity are related to the lattice dynamics, understanding the phonon thermal conductivity is also helpful to account for the damage mechanism, which motivates us to study phonon thermal conductivity of alpha-zirconium.

In fact, MD simulation has been a useful method to study thermal conductivity by phonons.[7–19] The anisotropy of thermal conductivity,[15] interface effect,[9,16] and size effect[7,10,11] on thermal conductivity were specially discussed. In MD simulations, the thermal conductivity can be computed either using equilibrium MD (EMD)[13,16,20,21] or non-equilibrium MD (NEMD).[7,9–11,14,16–19] Relatively, the NEMD method provides direct information about transport phenomenon.[7,22] So in this paper, the phonon conductivity of alpha-zirconium is theoretically estimated using the NEMD

*Project supported by the National Basic Research Program of China (Grant No. 2010CB731601).

†Corresponding author. E-mail: wslai@tsinghua.edu.cn

© 2013 Chinese Physical Society and IOP Publishing Ltd

method. The rest of this paper is organized as follows. The simulation model and method, including the empirical many-body potential and the calculation of the heat flux and the temperature gradient, are given in Section 2, and the results and discussion are presented in Section 3. Finally, some conclusions are drawn from the present study in Section 4.

2. Model and method

The thermal conductivity can be obtained by Fourier's law as

$$\kappa = -\frac{J}{\partial T/\partial X}, \tag{1}$$

where J is heat flux along a special orientation and $\partial T/\partial X$ is the gradient of the temperature along the heat flux. A simple nonequilibrium molecular dynamics method of calculating the thermal conductivity was presented in Ref. [23]. In this study, the phonon thermal conductivity is simulated using this method.

The empirical embedded atom method (EAM) potential of #3 given by Mendelev and Ackland[24] for alpha-zirconium is employed in the present study. The total energy is given by

$$U = \sum_{i=1}^{N-1} \sum_{j=i+1}^{N} V(r_{ij}) + \sum_{i=1}^{N} F(\rho_i), \tag{2}$$

where the subscripts i and j run over all atoms in the system, r_{ij} is the separation between atoms i and j, $V(r)$ is a pairwise potential, $F(\rho)$ is the embedding energy function and

$$\rho_i = \sum_j \Phi(r_{ij}), \tag{3}$$

where $\Phi(r)$ is the electron density contributed to i site from j atom.

Before starting the simulation of thermal conductivity, we first investigate the thermal expansions of alpha-zirconium at different temperatures. Figure 1 shows the sketch of a cell for constructing the simulated block. The simulated block contains 4000 atoms in $10 \times 10 \times 10$ cells, with period boundary condition used in x, y, and z axes along the $[2\bar{1}\bar{1}0]$, $[01\bar{1}0]$, and [0001] directions respectively. The simulations are carried out in the constant temperature — constant pressure (Nose–Parrinello–Rahman) ensemble,[25–27] and a fourth–order predictor-corrector algorithm[28] is used to integrate the equations of motion, in time steps of 2 fs. The pressure is set to be standard atmospheric pressure, and the target temperatures are set to be in a range from 200 K to 800 K. The total simulation time is 0.1 ns, which is enough to obtain a steady state of the system. Figure 2 shows the variation of average atomic volume with temperature. From the volume–temperature curve, the volume-expansion coefficients at various temperatures are determined to be 17.88×10^{-6}, 21.76×10^{-6}, and 25.62×10^{-6} K^{-1} at 600, 700, and 800 K, respectively, compared with the corresponding experimental values of 20.38×10^{-6}, 21.32×10^{-6}, and 22.22×10^{-6} K^{-1}.[29] It is seen that the potential of Zr used here can reproduce well the thermal expansion in the temperatures ranging from 500 K to 800 K, which are compatible to the experimental results. However, it predicts the expansion coefficient of 6.1×10^{-6} K^{-1} at 300 K compared with the experimental value of 17.35×10^{-6} K^{-1}, showing obvious deviation at low temperature from the experimental results. Thus we limit our study on thermal conductivity at the temperatures higher than 450 K, and use the equilibrium cell parameters determined here for the further simulation of thermal conductivity

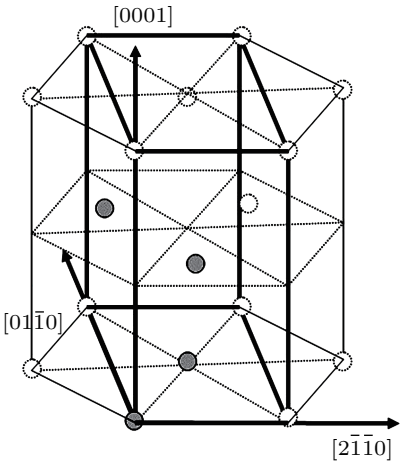


Fig. 1. A sketch of a cell for constructing the simulated block. The cuboid constituted by thick lines, containing four atoms, is one cell.

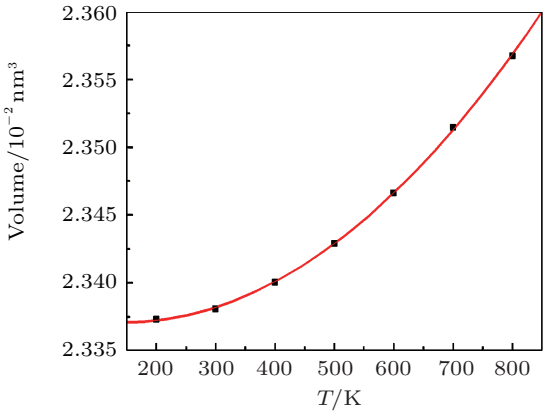


Fig. 2. Average atomic volume of Zr versus temperature.

2.1. Establishment of heat flux

In order to obtain a heat flux profile and a temperature profile, the simulation box is divided into N layers perpendicular to the heat flux orientation as shown in Fig. 3.[23] We simply take the coldest atom in the hot slab (slab $N/2$) and the hottest atom from the cool slab (slab 0), and then exchange their velocities to generate the heat flow. The kinetic energy distributions of the two slabs are wide enough so that the hottest atom of the cool slab is always found to have more

kinetic energy than the coldest atom of the hot slab. A temperature gradient in the middle region will be established after a certain amount of energy has exchanged between cool and hot slabs. After reaching a steady state, the exchanged energy is exactly balanced by the opposite heat flow.

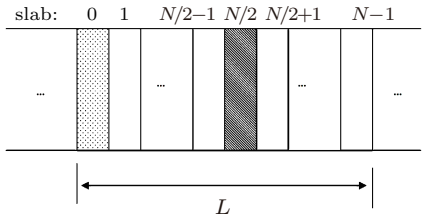


Fig. 3. Dividing the periodic simulation box into slabs. Slab 0 is the "cool" slab and slab $N/2$ is the "hot" slab.

Then the heat flux is calculated by

$$J = \frac{\Delta\varepsilon}{2AWt_{\mathrm{MD}}}, \tag{4}$$

where $\Delta\varepsilon$ is the average kinetic energy difference between the two atoms exchanged every W steps (heat exchange frequency) after reaching a steady state, t_{MD} is the time interval of MD step, and A is the area of the slabs. The factor of 2 in the formula arises from the symmetry of the arrangement (Fig. 3), and energy can flow from the hot slab to the cold slab in two directions, effectively doubling the area available for the flux.

To validate the above method applicable for Zr studied here, we first check whether the steady state can be established by exchanging atomic energy. The simulated system consists of 7680 atoms in a periodic supercell of $8 \times 6 \times 4$ cells. The direction of heat flux is along [0001] crystallographic orientation, W is chosen to be 25, and the target temperature is 700 K. The total simulation time is 0.6 ns (3×10^5 MD steps), which is needed because phonon–phonon scattering events in a solid are far less frequent than in a fluid of comparable density.[9] Figure 4 gives the variation of accumulated heat exchange energy (ε) with time. It can be seen that the exchange energy and time are well related to each other linearly, which means that the heat flux is constant and the simulation of thermal conduction is in a steady state.

2.2. Calculation of temperature gradient

When the system reaches a steady state, heat flux can be determined exactly by Eq. (4). Then it needs to determine the temperature gradient so as to calculate the thermal conductivity by Eq. (1).

According to the theory of the statistical mechanics, we can use equipartition theorem to determine the temperature (T) of slab k by

$$T_k = \frac{1}{3n_k k_{\mathrm{B}}} \sum_{i \in k}^{n_k} m_i v_i^2, \tag{5}$$

where n_k is the atomic number of the slab k, m_i the mass of the i-th atom in the slab k, k_{B} the Boltzmann's constant, and v_i the velocity of the i-th atom. Figure 5 shows the averaged temperature-z profile at four different simulation times, obtained by the simulation block the same as that in Fig. 4. It can be seen that the four temperature-z curves, performed for four different simulation times 0.3, 0.4, 0.5, and 0.6 ns, are almost the same, indicating that the system has achieved a steady state after 0.3 ns. It should be noted that in the slabs near the hot slab and the cool slab, a strong nonlinear phenomenon is seen, which contributes to the strong scattering caused by the heat source or heat sink.[7,9] In the middle region, temperature profile is linear and can be fitted by a straight line. As to the symmetry of the two middle regions, the slopes of the curves for the two different middle regions should be close to each other. The obtained values of 2.30354 and –2.36302 from Fig. 5 demonstrate that the thermal conduction of the two middle regions is symmetrical. Therefore, the temperature gradient can be determined from the temperature-z profile of the steady state by averaging right and left middle regions as expressed by

$$\partial T/\partial z = \frac{1}{2}(|\partial T/\partial z_{\mathrm{right}}| + |\partial T/\partial z_{\mathrm{left}}|). \tag{6}$$

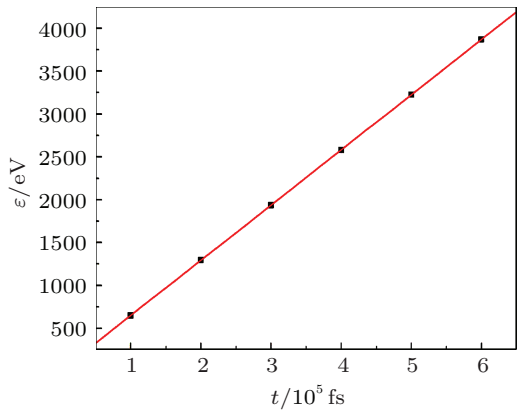


Fig. 4. Variation of the accumulated heat exchange energy (ε) with time obtained in the simulated block with the size of $8 \times 6 \times 40$ cells at 700 K.

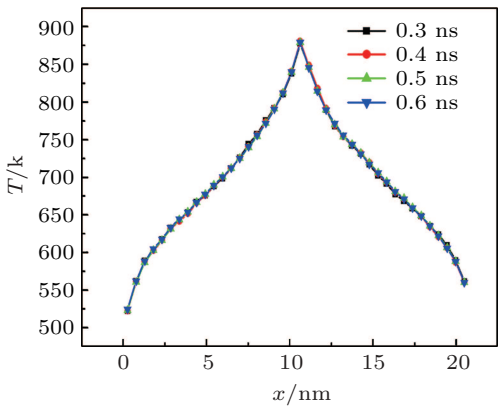


Fig. 5. Averaged temperature-z profiles at four different simulation times.

Then, based on Eq. (1), the phonon thermal conductivity can be computed. We will use the same calculation process in the other simulation conditions.

3. Results and discussion

3.1. Effect of heat exchange frequency

As introduced in Subsection 2.1 the interval W (heat exchange frequency) between atomic velocity exchanges governs the magnitudes of the heat flux and of the temperature gradient. To check its influence on the calculation of the phonon thermal conductivity, we choose $W = 25$, 40, 55, respectively to compute the phonon thermal conductivity along [0001] crystallographic orientation at 700 K. Figure 6 gives the variations of the accumulated heat exchange energy (ε) with time for different values of W. It can be seen that the curves are straight lines, suggesting that the steady heat flux has been established in all simulation systems. Accordingly the corresponding phonon thermal conductivities are calculated to be 2.073, 2.170, and 2.056 W/(m·K) respectively. It is seen that difference between those values appears to be small, indicating that the phonon thermal conductivity is almost insensitive to the heat exchange frequency. The similar results have also been reported in Ref. [7]. Therefore, we set $W = 25$ in the following simulations.

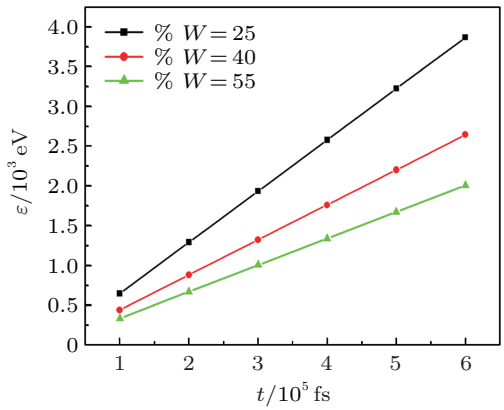


Fig. 6. Variations of the accumulated heat exchange energy (ε) with time for three different values of W.

3.2. Effect of finite size

When the dimension of the simulation systems along heat flux direction is not significantly longer than the phonon mean-free path, the effect of finite size on the phonon thermal conductivity will appear.[20,30] This can be explained by the scattering that occurs in the regions near the heat source and sink. Figure 7 shows the variations of the inverse of phonon thermal conductivity with the inverse of the dimension along heat flux [0001] direction at various temperatures. It can be seen that there exists a linear relationship between $1/\kappa$ and $1/L$, i.e.,

$$1/\kappa = s/L + b. \tag{7}$$

This linear relationship between $1/\kappa$ and $1/L$ of Eq. (6) has also been discussed in Refs. [7] and [30]. The phonon thermal conductivity of the infinite system is equal to the inverse of b, which can be obtained from Fig. 7 by extrapolating the fitting straight lines to $1/L = 0$. Thus, we obtain the phonon thermal conductivity of the infinite system by extrapolation to $1/L = 0$ in the later cases of the simulations. In order to do so, at least three computed blocks with the dimensions of 30, 40, 60 cells along the heat flux direction are employed in the simulations so that such an extrapolation could be done.

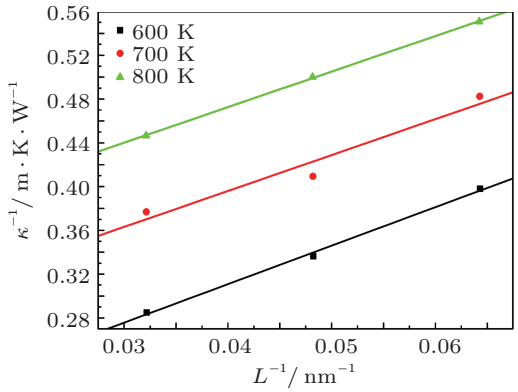


Fig. 7. Variations of the inverse of phonon thermal conductivity with the inverse of the dimension along heat flux [0001] direction at three different temperatures, showing a linear relationship between $1/\kappa$ and $1/L$, and very close slopes.

3.3. Effect of temperature

To investigate the variation of the phonon thermal conductivity with temperature, three simulation systems with the dimensions of $8 \times 6 \times 30$, $8 \times 6 \times 40$, $8 \times 6 \times 60$ cells, containing 5720, 7680, 11520 atoms respectively, are employed. In the simulations, the heat flux is along [0001] crystallographic orientation and the temperatures of the systems are set to be in a range from 600 K to 800 K. The calculated results of the phonon thermal conductivity are given in Table 1. It can be seen that κ decreases with the increase of temperature from 600 K to 800 K.

Table 1. Phonon thermal conductivities at different temperatures.

Temperature/K	Thermal conductivity/W·m^{-1}·K^{-1}
600	5.8734
700	3.7769
800	2.9174

According to the classical model, the phonon thermal conductivity is given by

$$\kappa = \frac{1}{3} c \bar{v}_{\mathrm{p}} l, \tag{8}$$

where c is the lattice heat capacity, $\bar{v}_{\mathrm{p}}$ the average speed of phonon movement, and l the phonon mean free path.[31] In fact, as temperature increases, the average number of phonons

and the probability of mutual collision between phonons increase, resulting in the decrease of the phonon mean free path. Furthermore, the lattice heat capacity at high temperature is almost independent of temperature. Thus, thermal conductivity will increase with temperature decreasing.[31] In Ref. [32], the author pointed out that such a trend is mainly due to enharmonic effect that becomes predominant at high temperature. The same phenomenon was found in Refs. [7], [20], and [21]. Through examining Table 1, the quantitative dependence of $T^{-2.443}$ (namely, $\kappa \propto T^{-2.443}$) can be found.

In the literature, it was found that the total thermal conductivity of zirconium (in $\mathrm{W{\cdot}m^{-1}{\cdot}K^{-1}}$) can be given by the recommended equation[33] in a temperature range from 298 K to 2000 K as

$$\kappa_{\text{total}} = 8.8527 + 7.0820 \times 10^{-3} T + 2.5329 \times 10^{-6} T^2 + 2.9918 \times 10^{3} T^{-1}, \quad (9)$$

which gives $\kappa_{\text{total}} = 16.5133$ at $T = 800$ K. It can be deduced that the present phonon thermal conductivity of single crystal is about 17.67 percent of the total thermal conductivity at this temperature. As the total thermal conductivity consists of electron and phonon thermal conductivity, the above results indicate that the electron thermal conductivity makes the main contribution to the total thermal conductivity, which is a common case for metals and alloys.

3.4. Anisotropy of thermal conductivity

We now analyze the influence of the anisotropy of the crystallographic orientation on phonon thermal conductivity. We choose three orientations $[2\bar{1}\bar{1}0]$, $[01\bar{1}0]$, and [0001] as heat flux direction, respectively. The case of [0001] crystallographic orientation has been discussed in the above section. For $[2\bar{1}\bar{1}0]$ crystallographic orientation, the dimensions of the simulated block are $30\times6\times8$, $40\times6\times8$, $60\times6\times8$ cells with the numbers of atoms being 5720, 7680, 11520, respectively. As for $[01\bar{1}0]$ crystallographic orientation, the simulated block includes $8\times30\times6$, $8\times40\times6$, $8\times60\times6$ cells and consists of 5720, 7680, 11520 atoms, respectively. The simulations are performed at 700 K. The calculated results are given in Table 2. It can be seen that the phonon thermal conductivity has different values for different crystallographic orientations and that maximum occurs along the direction perpendicular to the close-packed (0001) plane while the other two directions have the values of κ close to each other.

Table 2. Phonon thermal conductivities along different crystallographic orientations.

Crystallographic orientation	Thermal conductivity/$\mathrm{W{\cdot}m^{-1}{\cdot}K^{-1}}$
$[01\bar{1}0]$	2.8345
$[2\bar{1}\bar{1}0]$	2.6661
[0001]	3.7769

As the phonon thermal conductivity is correlated with transport of lattice vibration waves, we discuss a possible reason for the occurrence of anisotropy of κ. According to Debye's model, the circular frequencies of all lattice vibration waves obey $\omega = v_s K$, where v_s is the group velocity of wave along the wave vector K direction. In the Debye's model, it was assumed that v_s was equal to the velocity of sound, which is the velocity of the longitudinal acoustic wave of long wavelength. In solid, the velocity of sound is given by

$$v_s = \sqrt{\frac{Y}{\rho}}, \quad (10)$$

where Y is the elastic modulus and ρ the density of solids. It was reported that the elastic modulus of zirconium is 1.24×10^5 MPa in [0001] direction, and 1.04×10^5 MPa in both $[2\bar{1}\bar{1}0]$ and $[01\bar{1}0]$ directions.[34] Thus, we deduce $v_s = 4371$ m/s along the [0001] direction and $v_s = 4003$ m/s along the other directions. Accordingly, the largest v_s along [0001] direction indicates the fastest energy transportation of lattice vibration wave along this direction, for the group velocity represents the velocity of energy transportation of wave. Thus the largest κ along the [0001] direction is ascribed to the largest group velocity of lattice vibration wave along this direction. It is therefore concluded that the anisotropy of κ is due to the anisotropy of the group velocities of lattice vibration waves in different crystallographic orientations.

3.5. Effect of grain boundary

We now discuss the effect of grain boundary (GB) on the phonon thermal conductivity. Figure 8 shows the sketch of the simulated block containing Σ7 grain boundary. It can be seen that the simulated block consists of two parts, the left and the right. The three crystallographic orientations of the left part are $[2\bar{1}\bar{1}0]$, $[01\bar{1}0]$, and [0001], while they are $[13\bar{1}\bar{1}\bar{2}0]$, $[35\bar{8}0]$, and [0001] in the right part. The left part contains $7\times41\times8$ cells, and the right part has $1\times5\times8$ constructed cells. The total number of atoms in the simulated block is 17072. Considering the symmetry, we put the hot slab in the middle of the left part, and the cool slab in the middle of the right part.

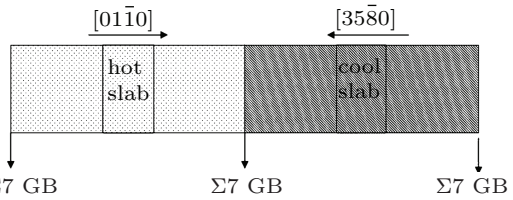


Fig. 8. Sketch diagram for the simulated block with grain boundaries.

The simulation condition is similar to that in the above section. The calculated averaged temperature y curve is given in Fig. 9. It can be obviously seen that a sharp drop of temperature across the GB occurs. The same phenomenon was

found in the simulation of heat flux across Si grain boundary in Ref. [9]. It should be noted that the average temperatures in the two regions are different, i.e., the average temperature is 717.47 K in the left and in the right it is 468.17 K. Apparently, the heat fluxes in the two regions are the same when the steady state has been established. The phonon thermal conductivities are calculated to be 2.3105 W/m·K and 3.8302 W/m·K for the left and right parts, respectively. The large value of κ of the right part as compared with that of left part, is due to the lower average temperature in the right part.

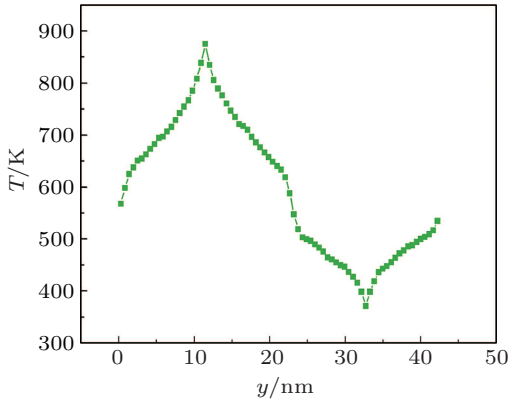


Fig. 9. Averaged temperature y profile for the simulated block with grain boundaries.

From the temperature y curve in Fig. 9, we can see a grain boundary phase with four or five slab thickness values at about 550 K in the GB region. The temperature gradient is relatively large, with a value of 71.7951 K/nm. Accordingly, the phonon thermal conductivity near GB is 0.6212 W/m·K. Additionally, we calculate the phonon thermal conductivity in the $[01\bar{1}0]$ crystallographic orientation at about 550 K and obtain the value of 5.2127 W/m·K in the bulk of single crystal. The phonon thermal conductivity near GB is only 12% of that in the bulk at the same temperature. We can use the ratio of the temperature discontinuity of GB and the heat flux to characterize the thermal/Kapitza resistance of a GB ($R_{\rm GB}$)[35] as follows:

$$R_{\rm GB} = \frac{\Delta T_{\rm GB}}{J}. \tag{11}$$

Therefore, we can obtain $R_{\rm GB} = 2.2 \times 10^{-9}$ m^2·K·W^{-1}, which is comparable to the thermal resistances of the GBs ranging from 10^{-10} m^2·K·W^{-1} to 10^{-9} m^2·K·W^{-1} reported by other simulations.[35] From the above analysis, we can conclude that in the crystal, the GB may act as a thermal barrier with low thermal conductivity.

4. Conclusions

In this paper, we study the phonon thermal conductivity using the NEMD method. The influences of different factors, including heat exchange frequency, finite size, temperature, crystallographic orientations, and grain boundary, on the simulated phonon thermal conductivity are considered. The simulation results indicate that heat exchange frequency has no significant influence on κ. The finite size of the simulation system has an effect on κ, and that there exists the linear relationship between $1/\kappa$ and $1/L$, which can be used to deduce κ of infinite system through extrapolation to $1/L = 0$. The phonon thermal conductivity is found to decrease with the increase of temperature. Anisotropy of κ is observed, which is due to the different group velocities of lattice vibration waves along different crystallographic orientations. In the region near GB, there is a sharp temperature drop, and the phonon thermal conductivity is about one-tenth of that in the bulk of single crystal at 550 K, suggesting that the GB may act as a thermal barrier in the crystal.

References

[1] Wooding S J, Howe L M, Gao F, Calder A F and Bacon D J 1998 *J. Nucl. Mater.* **254** 191
[2] Gao F, Bacon D J, Howe L M and So C B 2001 *J. Nucl. Mater.* **294** 288
[3] Wooding S J and Bacon D J 1997 *Philosophical Magazine A* **76** 1033
[4] Yamanaka S, Yamada K, Kurosaki K, Uno M, Takeda K, Anada H, Matsuda T and Kobayashi S 2002 *J. Nucl. Mater.* **294** 94
[5] Tsuchiya B, Huang J, Konashi K, Teshigawara M and Yamawaki M 2001 *J. Nucl. Mater.* **289** 329
[6] Raabe D, Xiang J Z and Wu X H 2002 *Computational Materials Science* (Beijing: Chemical Industry Press) p. 60 (in Chinese)
[7] Schelling P K, Phillpot S R and Keblinski P 2002 *Phys. Rev. B* **65** 144306
[8] Xia R H, Tian X G and Shen Y P 2010 *Acta Mech. Sin.* **26** 599
[9] Maiti A, Mahan G D and Pantelides S T 1997 *Solid State Commun.* **102** 517
[10] Heino P and Ristolainen E 2003 *Microelectron. J.* **34** 773
[11] Wang Z H and Li Z X 2006 *Appl. Therm. Eng.* **26** 2063
[12] Wagner G J, Jones R E, Templeton J A and Parks M L 2008 *Comput. Methods Appl. Mech. Eng.* **197** 3351
[13] Kaburaki H, Li J and Yip S 1999 *Mater. Res. Soc.* **538** 503
[14] Maeda A 1995 *Phys. Rev. E* **52** 234
[15] Mingo N, Yang L, Li D and Majumdar A 2003 *Nano Lett.* **3** 1713
[16] Abramson A R, Tien C L and Majumdar A 2002 *J. Heat Transfer* **124** 963
[17] Gu X K and Cao B Y 2007 *Chin. Phys.* **16** 3777
[18] Zhang M P, Zhong W R and Ai B Q 2011 *Chin. Phys. B* **20** 100508
[19] Fu B Q, Lai W S, Yuan Y, Xu H Y and Liu W 2012 *J. Nucl. Mater.* **427** 268
[20] Volz S G and Chen G 1999 *Physica B* **263** 709
[21] Volz S G and Chen G 1999 *Appl. Phys. Lett.* **75** 2056
[22] Ikeshoji T and Hafskjold B 1994 *Mol. Phys.* **81** 251
[23] MullerPlathe F 1997 *J. Chem. Phys.* **106** 6082
[24] Mendelev M I and Ackland G J 2007 *Phil. Mag. Lett.* **87** 349
[25] Nose S 1984 *J. Chem. Phys.* **81** 511
[26] Parrinello M and Rahman J 1981 *Appl. Phys.* **52** 7182
[27] Nose S and Klein M L 1983 *Mol. Phys.* **50** 1055
[28] Gear C W 1966 *ANL Report*, No. ANL-7126
[29] Goldak J, Lloyd L T and Barrett C S 1966 *Phys. Rev.* **144** 478
[30] Oligschleger C and Schön J C 1999 *Phys. Rev. B* **59** 4125
[31] Shen Y F 2005 *Basic Course of Solid State Physics* (Beijing: Chemical Industry Press) p. 260 (in Chinese)
[32] Castejon H J 2003 *J. Phys. Chem. B* **107** 826
[33] Fink J K and Leibowitz L 1995 *J. Nucl. Mater.* **226** 44
[34] Chen H, You S W, Hu Y F and Lü Y H 1993 *Rare Metal Mater. Eng.* **22** 67 (in Chinese)
[35] Crocombette J P and Gelebart L 2009 *J. Appl. Phys.* **106** 083520